

Late afterglows of GW/GRB 170817A

Houri Ziaeepour^{a,b}

^aInstitut UTINAM, CNRS UMR 6213, Observatoire de Besançon, Université de Franche Compté, 41 bis ave. de l'Observatoire, BP 1615, 25010 Besançon, France

^bMullard Space Science Laboratory, University College London, Holmbury St. Mary, GU5 6NT, Dorking, UK

E-mail: houriziaeepour@gmail.com

Abstract. The gamma-ray burst that followed the first detection of gravitational waves from the merger of a Binary Neutron Stars (BNS) and its low energy counterparts were in many respects unusual and challenge our understanding of mechanisms involved in their production. In a previous work we used a phenomenological formulation of relativistic shocks and synchrotron emission to analyse the prompt gamma-ray emission of GW/GRB 170817A. Here we use the same model to analyse late afterglows of this event. The main goal is to see whether synchrotron emission alone can explain the late afterglows. We find that collision between a mildly relativistic outflow from the merger with a Lorentz factor of $\sim 1.2 - 3$ and the ISM/circumburst material can explain observations, if the synchrotron self-absorption of radio emission and local extinction of optical/IR photons are taken into account. In absence of a significant extinction, an additional source of X-ray is necessary to explain the data. These conclusions are in large extend independent of the model used here and can be deduced directly from data. We also show that at the time of its encounter with circumburst material the outflow could have been still mildly magnetized. The origin for optical extinction could be a dust rich old faint star cluster surrounding the BNS, which additionally had helped its formation and merger. Such an environment evades present observational constraints and is consistent with our conclusions about properties and evolution of the progenitor neutron stars obtained from analysis of the prompt gamma-ray emission. Alternatively, if the synchrotron emission was produced internally through collisions of density shells, the extinction might have occurred inside the outflow itself rather than externally. The most plausible additional source of X-ray is the decay of medium and heavy isotopes produced by the kilonova, including r-processes, and the recombination of cooled electrons. The contribution of these processes should be quantified in future works.

Keywords: gamma-ray burst, gravitational wave, binary neutron star, merger

Contents

1	Introduction	1
2	Model	2
3	Late afterglow of GW/GRB 170817A	3
3.1	Initial conditions	5
4	Simulations	6
4.1	Absorption	8
5	Discussion	9
6	Outlines	12
A	Synchrotron self-absorption	13
B	Evolution models of active region	14

1 Introduction

The afterglow of GRB 170817A associated to the Gravitational Wave (GW) event GW 170817 is the only short GRB with very long follow up in a broad band of energies, from X-ray to radio. The motivation for studying these faint emissions is not only investigating the fate of a Binary Neutron Star (BNS) merger remnant, but also understanding the origin of unusual faintness of the prompt gamma-ray emission of this event and peculiar behaviour of its afterglows, namely their early faintness and late brightening¹. Explanations suggested in the literature include: off axis observation of both prompt and afterglow of an otherwise ordinary short GRB [42, 49, 62, 87, 88]; prompt gamma-ray emission from breakout of a choked jet and afterglow from a mildly relativistic² structured jet [47, 53] or a cocoon [16, 33, 40, 60, 63, 65, 70]; prompt emission from a structured jet and afterglow from a roughly spherical outflow [56, 58]; and variation of these models: jet breakout from wind [72], jet-merger-ejecta interaction [43], neutron-rich isotropic fireball [76], and gamma-ray emission from a wide spiraling outflow [25].

Predictions of these models have been mostly compared only with late X-ray and radio afterglows, because no observation in these bands was performed before $\sim T + 1.6$ days, where T is the Fermi-GBM [19] trigger time. No counterpart was detected before $\sim T + 10$ days and $\sim T + 16$ days in X-ray and radio wavelengths, respectively. The earliest observations in optical/IR began at the same time as in X-ray and radio, and led to the detection of a counterpart. However, emissions in optical/IR bands are

¹In this work by *early afterglows* we mean emissions in X-ray and lower energy bands from $\gtrsim 70$ sec - the average slew delay of the Neil Gehrels Swift Observatory [29] - up to $\mathcal{O}(1) \times 10^5$ sec, i.e. a couple of days after gamma-ray trigger. This is the time interval in which the afterglow of most short GRBs detected by the Swift have been observed. Usually no later attempt is made to detect afterglows of GRBs without an X-ray counterpart in this interval and GRB 170817A is an exception.

²In the literature the range of Lorentz factor called *mildly relativistic* varies and depends on the context and author. Here we use this term for fluids with a Lorentz factor in the range of 1.2 – 5, corresponding to velocity range $0.5c - 0.98c$, where c is the speed of light.

believed to be dominated by a kilonova originated from the ejection of hot low velocity material from the disk/torus of the merger [3, 5, 12, 14, 39, 59, 66, 81] and not from the GRB producing jet. Nonetheless, a contribution from the polar outflow, which generates a relativistic jet and a GRB may be necessary to explain these observations [3, 81]. We remind that most works on the unusual properties of GRB 170817A do not compare their models with the prompt emission data obtained by the Fermi-GRB [31] and the Integral-IBIS [79] instruments, and only their consistency with the data is discussed.

In a previous work [94] we used a phenomenological formulation of relativistic shocks and their synchrotron/self-Compton emission [92, 93] to model in detail light curves and spectrum of the prompt gamma-ray emission of GRB 170817A. It shows that the most plausible Lorentz factor for the relativistic jet of this burst is $\Gamma \sim 100$. However, parameters of the model are degenerate and a low Lorentz factor of ~ 10 also fits the data, if the energy transfer to accelerated electron is very efficient and close to highest values seen in Particle In Cell (PIC) simulations [83]. In any case, these Lorentz factors are in the highest limit of values suggested in the literature, but at least few folds less than what is predicted for more typical short GRBs, for instance GRB 130603B [57] which was also associated to a kilonova [5, 85]. Moreover, it is found that density and extent of the relativistic jet of GRB 170817A were more than an order of magnitude less than GRB 130603B. Using the results of BNS merger simulations, we concluded that plausible reasons behind the weak jet in GW 170817 BNS merger event were: the old age of neutron star progenitors and their reduced magnetic field and consequently availability of less energy for formation and acceleration of the jet; the closeness of progenitors masses; and finally the evolutionary history of the BNS and perturbation of its orbit and spin of neutron stars due to encounter with other stars and gravitational disturbances, probably in the dense environment of a star cluster. These event misaligned spins of neutron stars and along with reduced magnetic fields of stars led to a weaker than usual polar dynamical ejecta during merger.

To complete our analysis of GW/GRB 170817A electromagnetic data, in this work we present simulations of late afterglows according to the same phenomenological model as the one used for the modelling of prompt emission. Several groups have used approximate analytical expressions for synchrotron emission from shocks to fit light curves of afterglows of GW/GRB 170817A [36, 60, 65, 88], and obtain good fit to the data. In this approach models used for fitting the data depend on a few parameters and it is not difficult to obtain an acceptable fit by adjusting them. Even in works based on MHD simulations such as [36], the MHD is used to predict properties of the outflow such as its kinetic and density rather than the observed synchrotron emission. Therefore, a goal of present work is to see whether simulation of shocks and synchrotron emission using physically motivated expressions for fundamental quantities such as densities, magnetic field, etc. confirm the prior assumption of synchrotron emission as origin of afterglows, or contribution from other processes would be needed to explain the data. Considering the complexity of the physics of BNS merger and its remnants, it is expected that after weakening of shocks in the ejecta, subdominant processes such as decay of long living isotopes in the kilonova remnant become detectable.

We briefly review the model and its parameters in Sec. 2. Methodology of modelling, initial conditions, and assumptions are discussed in Sec. 3. Results of the simulations are presented in Sec. 4. Interpretation of the results are discussed in Sec. 5, and outlines in Sec. 6. In Appendix A we calculate synchrotron self-absorption index for the phenomenological shock model of [92, 93]. Appendix B summarizes phenomenological expressions used for modelling the width of synchrotron emitting region in the model.

2 Model

The phenomenological model of [92, 93] assumes that GRB emissions are produced by synchrotron/self-Compton processes in a dynamically active region in the head front of shocks between density shells inside a relativistic cylindrical jet for prompt and with surrounding material for afterglows in lower energies. In addition to the magnetic field generated by Fermi processes in the active region an external magnetic field precessing with respect to the jet axis may contribute in the production of synchrotron emission. An

essential aspect of this model, which distinguishes it from other phenomenological GRB formulations, is the evolution of parameters with time. Moreover, simulation of each burst consists of a few time intervals - *regimes* - each corresponding to an evolution rule (model) for phenomenological quantities such as: fraction of kinetic energy transferred to fields and its variation; variation of the thickness of synchrotron/self-Compton emitting *active* region; etc. Division of simulated bursts to these intervals allows to change parameters and phenomenological evolution rules which are kept constant during one time interval. Physical motivation for such fine-tuning is the fact that GRB producing shocks are in a highly non-equilibrium and fast varying state. In fact, multiple variation of the slope of afterglows light curves, which presumably are produced by external shocks on the ISM or circumburst material is an evidence that they are not completely uniform and their anisotropies affect the emission.

This simplified formulation of shocks is originally constructed for prompt and early afterglow emissions, which presumably are generated by a fast and compact ejecta. The main approximation in the model is the assumption that properties of matter in colliding shells is uniform and self-similar. According to this approximation the evolution of shock and its synchrotron emission depends only on time or equivalently distance from the center, rather than to both time and distance as independent variables. However, as suggested in the literature [17, 33, 36, 40, 60] and we give more arguments in its favour in the next section, the observed late afterglows of GW/GRB 170817A might have been produced by a continuous flow with varying spatiotemporal characteristics. To take into account slow variation of characteristics of the outflow, we simulate the model with different densities and speeds, presenting slow variation of physical properties. Each simulation can be considered as presenting the outflow at different epochs or fraction of material with corresponding properties. If the underlying priors are correct, a linear interpolation between these models should be a good approximation of emission from a slowly varying or nonuniform outflow.

Table 1 summarizes parameters of the model. Despite their long list, simulation of typical long and short GRBs in [93] shows that the range of values which lead to realistic bursts are fairly restricted. Evidently, the range of some parameters for simulation of prompt and afterglow are very different. In particular, we assume that the ISM or surrounding material is at rest with respect to a far observer at the same redshift. They are non-relativistic and in comparison with relativistic outflows their velocity dispersion is negligible. Therefore, for external shocks the Lorentz factor of slow shell Γ is always 1.

3 Late afterglow of GW/GRB 170817A

It is unlikely that the observed electromagnetic emissions from GW/GRB 170817A event at $\gtrsim T + 10$ days can be due to the remnant of the relativistic jet which generated the observed prompt gamma-ray. The early afterglows of short GRBs, which are presumably produced by weaker internal and external shocks of the relativistic jet [91], are usually observable for few days, because their flux declines very quickly in all bands [38]. Therefore, as other authors concluded [17, 56, 60], at $\gtrsim T + 10$ days the relativistic jet of GRB 170817A, which according to our analysis its kinetic energy, extent, and density were much smaller than typical short GRBs [94], has been weakened and dissipated by interaction with its surrounding material [93] and could not have significant contribution in the observed emissions. In this case, it would be indistinguishable from the slower part of dynamical ejecta.

The observed late brightening of GRB 170817A and a few other short [26, 68] and long [15, 18] GRBs should be due to the emission from other components of ejecta and/or other processes. Candidates suggested in the literature are: MHD instabilities leading to increase in magnetic energy dissipation [4, 6]; external shocks generated by the collision between the ISM or circumburst material and a mildly relativistic thermal cocoon ejected at the same time as the ultra-relativistic component and lagged with respect to the jet [16, 36, 53, 64]; late outflows from a long lasting accretion disk [61]; fall-back of ejected matter to the central black hole [52].

The off-axis view of a structured jet predicts late brightening of afterglows [42, 48, 49, 56]. However, the observed decline of X-ray flux at $\lesssim T + 134$ days [17] is inconsistent with simulations of significantly off-

Table 1. Parameters of the phenomenological relativistic shock model

Model (mod.)	Model for evolution of active region with distance from central engine; See Appendix B and [92, 93] for more details.
r_0 (cm)	Initial distance of shock front from central engine.
Δr_0	Initial (or final, depending on the model) thickness of active region.
p	Slope of power-law spectrum for accelerated electrons; See eq. (3.8) of [93].
p_1, p_2	Slopes of double power-law spectrum for accelerated electrons; See eq. (3.14) of [93].
γ_{cut}	Cut-off Lorentz factor in power-law with exponential cutoff spectrum for accelerated electrons; See eq. (3.11) of [93].
γ'_0	Initial Lorentz factor of fast shell with respect to slow shell.
δ	Index in the model defined in eq. (3.29) of [93].
Y_e	Electron yield defined as the ratio of electron (or proton) number density to baryon number density.
ϵ_e	Fraction of the kinetic energy of falling baryons of fast shell transferred to leptons in the slow shell (defined in the slow shell frame).
α_e	Power index of ϵ_e as a function of r .
ϵ_B	Fraction of baryons kinetic energy transferred to induced magnetic field in the active region.
α_B	Power index of ϵ_B as a function of r .
N'	Baryon number density of slow shell.
κ	Power-law index for N' dependence on r' .
n'_c	Column density of fast shell at r'_0 .
Γ	Lorentz factor of slow shell with respect to far observer.

- ★ The phenomenological model discussed in [92] and its simulation [93] depends only on the combination $Y_e \epsilon_e$. For this reason only the value of this combination is given for simulations.
- ★ The model neglects variation of physical properties along the jet or active region. They only depend on the average distance from center r , that is $r - r_0 \alpha t - t_0$.
- ★ Quantities with prime are defined with respect to rest frame of slow shell, and without prime with respect to central object, which is assumed to be at rest with respect to a far observer. Power indices do not follow this rule.

axis emission [49], which predict a break after a few hundred days. Other simulations, for instance those reported by [30, 56] predict earlier break, but cannot discriminate between off-axis and cocoon (structured jet) models [60] and need polarimetry and imaging to discriminate between them [30].

Our prior assumption is that late afterglows of GRB 17081A and their brightening is due to synchrotron emission from the mildly relativistic remnant of dynamical ejecta during BNS merger, which from now on we simply call *the outflow*. Indeed, General Relativistic Magneto-Hydro-Dynamic (GRMHD) simulations of BNS merger show poleward mildly relativistic - with a Lorentz factor of $\lesssim 4$ - mass ejection [20, 27, 44]. Only a small fraction of this ejecta is accelerated to ultra-relativistic velocities by the transfer of Poynting energy of the ejecta to kinetic energy [6, 45, 86]. The remaining material continues its trajectory and eventually collides with the ISM and/or circum-BNS material at a later time. If this scenario is correct, brightening of afterglows in other short GRBs is missed because observations were not sufficiently long.

GRMHD simulations show that the opening angle of this outflow is $\lesssim 30^\circ$. The orbit inclination of the BNS merger associated to GW 170817 is estimated as $\theta_w \lesssim 18^\circ - 27^\circ$ [54]. Therefore, the viewing angle is expected to pass through the outflow and even if the latter have a somehow non-uniform velocity profile [53],

in comparison with other uncertainties of the model its effect would be negligible for analysing the data. Indeed, the negligence of the inclination of the line of sight with respect to the outflows symmetry axis induces an error $\propto(1 - \cos \theta_w) \lesssim 8\%$ for $\theta_w \approx 20^\circ$ in the simulated light curves, which is much less than other uncertainties of the model. For this reason, we will not discuss the issue of viewing angle further. Nonetheless, due to these simplifications and degeneracies between parameters of the model discussed in details in [94], the estimation of characteristics of the outflow by simulations presented in the next section should be considered as *order of magnitude* rather *exact*.

Although observations of GRBs afterglows are consistent with synchrotron/self-Compton mechanism as the main emission process, subdominant processes may become important and observable when the main source weakens. In particular, following the observation of a kilonova [3, 13, 14, 39] in GW/GRB 170817A event, we know that the decay of isotopes produced during merger and recombination of cooled electrons contribute to the emissions.

3.1 Initial conditions

Before discussing how we have estimated initial conditions for the simulation of late afterglows of GRB 170817A we should remind that in the phenomenological model of [92, 93] the jet is cylindrical and as long as the line of sight of the observer pass through it and its Lorentz factor is sufficiently high such that $\sin \theta_j > 1/\gamma'$, the effect of oblique view is negligible³. Additionally, it is proved that for $\Gamma_j \gg 1$ the contribution of high latitude emission is small [92]. This condition is not fully satisfied by the late outflow, which is expected to be only mildly relativistic. Nonetheless, even for an outflow with a Lorentz factor $\Gamma_c \sim 2$ the value of $1/\Gamma_c^2 \sim 1/4 \sim 1/2\Gamma_c$. Considering other theoretical and observational uncertainties in the modelling of the data, this amount of error should be tolerable when the aim is order of magnitude estimation of physical quantities which characterize the outflow and material surrounding the BNS merger.

Initial values of some parameters in Table 2 cannot be arbitrarily selected. For instant, the initial distance of the jet front from center when the presumed external shock begins must be consistent with the value of outflow's β and the time of first detection of electromagnetic signal from outflow's external shock. For $\beta = 0.4$ and 0.8 corresponding to $\gamma' \approx 1.2$ and 2.34 ,⁴ the distance of the ejecta's front r_0 at the beginning of its collision with the ISM/surrounding material at $\lesssim 10$ days after merger must be $\approx 10^{16}$ cm and 2×10^{16} cm, respectively.

To estimate physically plausible column density of the outflow we use the results of GRMHD numerical simulations of BNS merger. The total amount of fast tail (dynamical) ejecta is expected to be $0.01 - 0.03 M_\odot$, where M_\odot is the solar mass [3, 69, 81]. In the case of GW 170817 event a larger ejecta of $m_{ejecta} \sim 0.03 - 0.05 M_\odot$ seems necessary to explain the bright UV/blue emission of kilonova at $\sim T + 1.6$ days [81]. However, a contribution from GRB 170817A afterglow in the early blue peak cannot be ruled out [3], see also the discussion about the early afterglow of this burst in [94]. We show later that under some conditions our simulations are consistent with the prediction of GRMHD simulations.

Using the above estimated ejecta mass, the baryon number column density at distance $r_0 = c\beta t_0$ can be parametrized as: $n'_c = 0.3 \times 10^{25} \eta A / \beta^2 t_{day}^2$, where $\eta \equiv \pi/\theta_c$ and $A \equiv m_{ejecta}/0.01 M_\odot$. We use the approximate time of the first detection of the X-ray counterpart $t_0 \sim 10$ days to estimate order of magnitude value of column density n'_c to be used in our simulations. For instance, for $\beta = 0.8$, $A = 1$, and a close to spherical outflow, we obtain $n'_c \sim 4.7 \times 10^{22}$ cm⁻² and $r_0 \sim 2 \times 10^{16}$ cm; for $\beta = 0.4$ the column density increases to $n'_c \sim 1.9 \times 10^{23}$ cm⁻² and initial distance decreases to $r_0 \sim 10^{16}$ cm. The values for distance to circumburst material found here correspond to typical distance of termination shock of ejecta from a star, that is where the ISM pressure becomes equal to wind pressure. In the cases of GW 170817 event

³For external shocks $\Gamma = 1$. Thus, relative Lorentz factor of shells γ' is equal to Lorentz factor of the jet Γ_j with respect to a far observer at the same redshift as the source.

⁴Because we assume that $\Gamma = 1$, i.e. the ISM/circumburst material is at rest with respect to a far observer at the same redshift, γ' is the Lorentz factor of jet with respect to observer. Nonetheless, we keep ' for consistency of notation with Table 1.

circumburst material should consist of pre-merger ejecta - presumably the remnant of ejected matter during and after the formation of neutron stars and BNS and/or accreted material from environment.

We should remind that due to the large parameter space of the model it was not possible to perform a systematic search for the best combination of parameters. This fact must be taken into account when simulations are compared with data and the values of parameters given in Table 2 should be considered as order of magnitude estimations.

4 Simulations

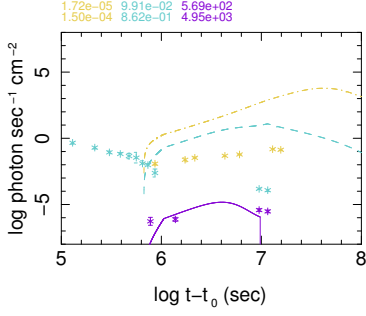
Fig. 1 shows simulations which reproduce well at least one of the 3 energy bands with late observations, namely X-ray, optical/IR and 6 GHz radio bands. Parameters of these simulations are shown in Table 2. We remind that only two relatively close in time data points are available in optical/IR band at late times⁵. Earlier data in this band is dominated by the kilonova emission and cannot be used to investigate the origin and properties of late emission, which as we discussed earlier, is presumably produced by other components of the ejecta from the BNS merger, in particular by a mildly relativistic outflow. Values of Lorentz factor (or equivalently β) chosen for these simulations, namely $\beta = 0.4, 0.8$ correspond to what is used in the literature for simulating late light curves of GW/GRB 170817. As we discussed in Sec. 2, we performed simulations with different Lorentz factor and flow density to mimic variation of outflow characteristics which couldn't be included in our simplistic model.

Simulations No. 1 and 2 are good fits to X-ray data, simulation No.3 fits X-ray and radio, and simulation No. 4 fits well optical and radio data. A main difference between simulations which fit X-ray data and those which fit radio data is the higher density of ISM/circum-merger material in the former with respect to the latter. They presumably present a denser front part, which collides with a denser circum-merger material, and a diluted hind part, which collides with the remnant of ISM/circum-merger material after its distortion and spread out by the front of the flow, respectively. A priori a linear interpolation between these simulations should lead to an acceptable fit of all three energy bands. However, it is easy to see that no linear combination of simulations fits all the light curves and either leads to over production of optical and radio emissions by the denser front part of the flow or under-estimation of X-ray. Indeed an interpolation in time between simulations with high and low Lorentz factors needs zero contribution from the denser part of outflow around the time of last X-ray observations to be consistent with optical observations at the same time.

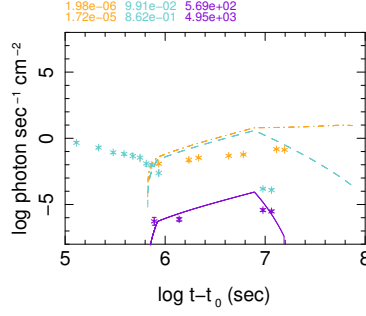
We also considered the effect of a Poynting flow imprinted in the outflow material. Ejected material from BNS merger is expected to be initially highly magnetized and may preserve part of its magnetic energy well after its expansion. Even in the case of main sequence stars such as the Sun a weak magnetic field is detected at upstream of wind termination shock [7]. Simulations No. 7 and 8 in Fig. 1 are examples of the case of a magnetically loaded outflow. Simulation No. 7 has the same parameters as Simulation No. 4, which fits radio and optical data well but has insufficient X-ray. We find that when a magnetic field with initial flux of $|B| \sim 5$ G is added to this model, both X-ray and optical emissions become much brighter than observations. Simulation No. 8 in Fig. 1 has the same parameters as model No. 7 in Table 2. It presents a more diluted outflow and circum-burst material but the same magnetic field as simulation No. 7. Fig. 1 shows that its X-ray light curve is consistent with the data. Moreover, the lower column density in this model is better consistent with the estimated value found in Sec 3.1. However, its optical emission is too bright and similar to simulations No. 1 to 3. Thus, only in presence of significant extinction the model this simulation can be consistent with data. In both these examples radio emission remains consistent with observations.

⁵At the time of preparation of this article new observations of GW 170817 counterpart in far-IR at $\sim T + 264$ days was published [89]. They are not considered in our analysis, partly to avoid further delay in the completion of our work and partly because far-IR emission at the epoch of observations is expected to be dominated by kilonova emission [89].

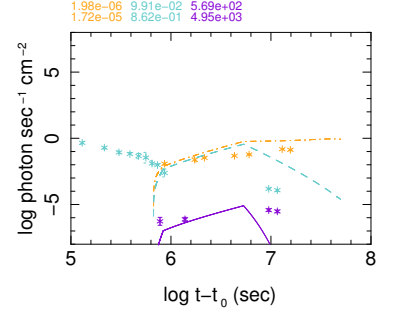
Simul. 1



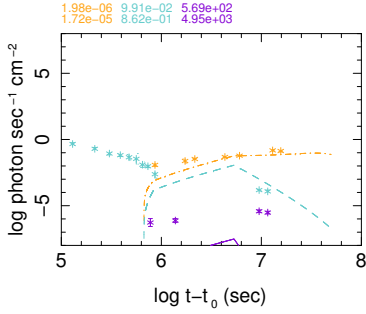
Simul. 2



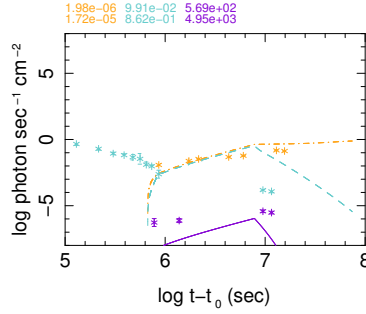
Simul. 3



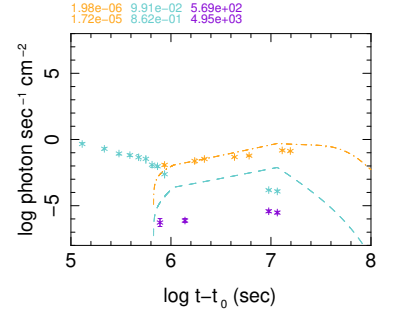
Simul. 4



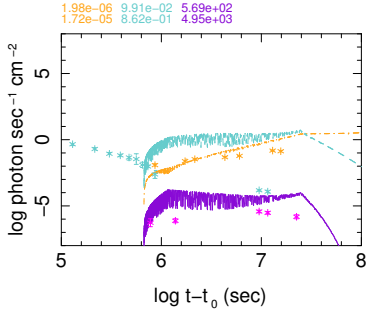
Simul. 5



Simul. 6



Simul. 7



Simul. 8

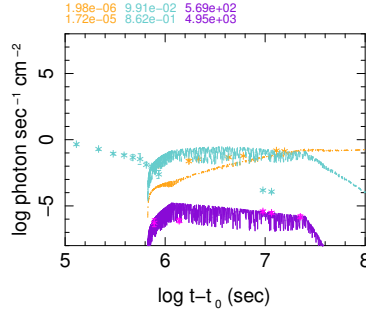


Figure 1. X-ray, optical, and radio light curves of simulated models without taking into account synchrotron self-absorption. The energy range for each band is written in the same colour/gray scale as the curve on the top of each plot. Stars present data taken from: [56] (X-ray), [17, 53, 69, 82] (optical), [1, 21, 35] (radio). Parameters of simulations No. 1 to 6 corresponds to models No. 1 to 6 in Table 2. Simulation No. 7 has the same parameters as simulation No. 4 but include an external magnetic field - presumably a Poynting flow oscillating with a frequency of 0.01 Hz and $|B| = 5(r/r_0)^{\alpha_m}$ G, where $\alpha_m = 1, 1, 2$ in the 3 regimes of this simulation. Simulation No. 8 corresponds to model No. 7 in Table 2 and includes an external magnetic field similar to that of simulation No. 7. Note that the plots of the last 2 simulations include X-ray observation by Chandra at $\sim T + 260$ days [67].

To explain discrepancies between data and simulated optical and radio light curves we first consider two important processes which are so far overlooked. They are synchrotron self-absorption in radio band and extinction of optical emission by material around the merger and in its environment.

Table 2. Parameter set of simulated models.

Simul. No.	mod.	γ'_0	r_0 (cm)	$\frac{\Delta r_0}{r_0}$	$(\frac{r}{r_0})_{max}$	p	γ_{cut}	κ	δ	ϵ_B	α_B	$\epsilon_e Y_e$	α_e	N' (cm ⁻³)	n'_c (cm ⁻²)
1	1	2.3	2.34×10^{16}	10^{-5}	1.5	1.8	100	-0.1	0.5	5×10^{-4}	-1	0.02	-1	0.5×10^3	10^{22}
	2	-	-	-	10	-	100	-0.4	0.1	-	0	-	0	-	-
	2	-	-	-	50	-	100	0	0.5	-	1	-	1	-	-
2	1	1.2	10^{16}	5×10^{-3}	1.5	1.8	100	-0.5	1	0.05	-1	0.1	-1	1	5×10^{23}
	2	-	-	-	15	-	100	0	0.1	-	0	-	0	-	-
	2	-	-	-	10	-	100	1	1	-	1	-	1	-	-
3	1	1.2	10^{16}	10^{-3}	1.5	1.8	100	-0.5	1	0.05	-1	0.1	-1	1	5×10^{23}
	2	-	-	-	10	-	100	0	0.1	-	0	-	0	-	-
	2	-	-	-	10	-	100	1	1	-	1	-	1	-	-
4	1	1.2	10^{16}	5×10^{-3}	1.5	2.1	100	-0.5	1	0.08	-1	0.1	-1	0.08	5×10^{23}
	2	-	-	-	10	-	100	0	0.1	-	0	-	0	-	-
	2	-	-	-	10	-	100	1	1	-	1	-	1	-	-
5	1	1.2	5×10^{16}	10^{-3}	1.5	2.5	100	-0.5	1	0.05	-1	0.1	-1	0.5	5×10^{23}
	2	-	-	-	10	-	100	0	0.1	-	0	-	0	-	-
	2	-	-	-	10	-	100	1	1	-	1	-	1	-	-
6	1	2.3	2.34×10^{16}	10^{-3}	1.5	1.8	100	-0.5	1	0.05	-1	0.02	-1	$1.e-1$	5×10^{22}
	2	-	-	-	10	-	100	0.2	0.1	-	0	-	0	-	-
	2	-	-	-	10	-	100	1.5	1	-	1	-	1	-	-
7	1	1.2	10^{16}	5×10^{-3}	2.5	2.1	100	-0.5	1	0.08	-1	0.1	-1	0.008	10^{22}
	2	-	-	-	30	-	100	0	0.1	-	0	-	0	-	-
	2	-	-	-	20	-	100	1	1	-	1	-	1	-	-

- ★ For external shocks of jet with the ISM or circumburst material $\Gamma = 1$ is assumed. In this case γ' is the Lorentz factor of jet with respect of a far observer at the same redshift.
- ★ Each data line corresponds to one simulated regime, during which quantities listed here remain constant or evolve dynamically according to fixed rules. A full simulation of a burst usually includes multiple regimes (at least two).
- ★ Horizontal black lines separate time intervals (regimes) of independent simulations identified by the number shown in the first column.
- ★ A dash as value for a parameter presents one of the following cases: it is irrelevant for the model; it is evolved from its initial value according to an evolution equations described in [92, 93]; or it is kept constant during all regimes.

4.1 Absorption

Low energy emissions are absorbed by gas and dust in circumburst material and ISM, and through synchrotron self-absorption process in the shocked region of the outflow. The main source of absorption for X-ray is neutral atomic gas. The H_I equivalent column density of the Milky Way N_H^{MW} in the direction of GW/GRB 170817A is $7.84 \times 10^{20} \text{ cm}^{-2}$ [55, 87]. Using 0.3-10 keV X-ray data from Chandra, the intrinsic column density in front of the ejecta of GW/GRB 170817A is estimated to be $\lesssim 3 \times 10^{22} \text{ cm}^{-2} \approx 0.05 \text{ gr/cm}^2$ [55, 87]. It presumably presents material in the local environment of the progenitor BNS and is much smaller than characteristic absorption length of 0.3-10 keV X-ray, which is $\sim 0.2 \text{ gr/cm}^2$ [84]. Thus, X-ray absorption is only a few percents [84] and negligible with respect to observational and modelling uncertainties.

In astronomical shocks synchrotron self-absorption is significant only in radio band [75]. In appendix A we calculate synchrotron self-absorption coefficient in the framework of phenomenological shock model of [92].

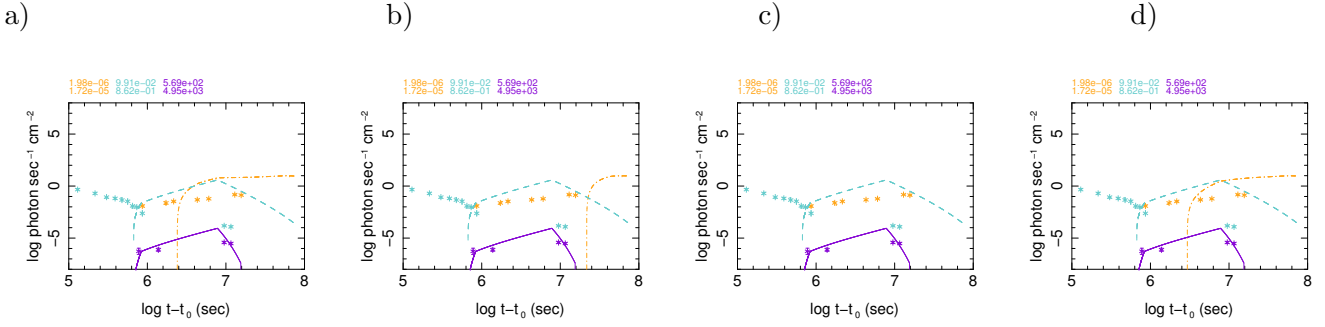


Figure 2. Light curves of Model No. 2 with different self-absorption length index α defined in Appendix A: Exponential dependence on distance and $\alpha = 1$ (a), $\alpha = 0.1$ (b), and $\alpha = 0$ (c); power-law dependence on distance and $\alpha = 3$ (d). Description of light curves and data is the same as Fig. 1

Plots in Fig. 2 show the effect of synchrotron self-absorption for simulation No. 2 and a phenomenological description for the variation of absorption length with propagation as an exponential or power-law, see Appendix A for details. They confirm that $\lesssim 6$ GHz radio emission can be completely absorbed if the extension of the induced magnetic field in front of the shocked region is enough long. Indeed, radio emission in both short and long GRBs is only observed at late times and well after the decline of higher energy counterparts. In the case of GW/GRB 170817A the first detection of a counterpart in radio was only a few days after the first detection in X-ray [1, 2, 21, 35, 60, 72]⁶. However, as it is explained in details in [94] we have most probably missed the early X-ray and optical afterglows. Assuming that the denser front of the outflow had a long effective length for synchrotron self-absorption, its radio emission was completely extinguished locally and what we observe comes from the weak shocks of slower (tail) component of the flow presented by simulations No. 4, 5, and 6 in Fig. 1.

Optical and IR bands are mainly affected by dust and electrons in the outer shells of neutral or slightly ionized atomic gas. The extinction in the Milky Way in the direction of GW 170817 is estimated to be only $A_V \lesssim 0.5$ mag [13]. Moreover, due to the very low star formation rate of the host galaxy NGC 4993, the extinction inside the host is believed to be negligible [12]. Therefore, any further extinction must be local and due to the circum-merger material and environment. As mentioned earlier, X-ray data shows the existence of an equivalent $N_H \lesssim 3 \times 10^{22} \text{ cm}^{-2}$ column of material in front of the outflow. If this material were genuinely hydrogen, it had negligible effect on the optical/IR emission. However, in the environment of old collapsed stars a large fraction of this material should consist of heavier elements such as *O*, *C*, *Fe*, *Si*, etc. [34]. They can significantly affect low energy photons if they are not fully ionized. Indeed, measurements of equivalent column density N_H and extinction A_V in supernovae remnants show a linear relation between $\log N_H$ and A_V , see e.g. [32, 71, 73]. A recent calibration of this relation in SNRs [34] estimates this relation as $N_H = (2.1 \pm 0.09) \times 10^{21} A_V \text{ (cm}^{-2}\text{)}$. Using this equation, we find that for $N_H \lesssim 3 \times 10^{22} \text{ cm}^{-2}$ the amount of extinction in visible band is $A_V \lesssim 10 \text{ mag} \sim 4 \text{ dex}$. This amount of extinction can make optical light curve of simulations No. 2, 3, and 8 fully consistent with the data.

5 Discussion

To generate a light curve consistent with observations we assumed a density profile for the ISM/circumburst material. An example of such profiles is shown in Fig. 3-a. It evolves with the distance from central object according to a power-law with index κ defined in Table 1. Its value for each model can be found in Table 2. This phenomenological model allows to determine the profile of circumburst matter dynamically. It was

⁶Observations in this work was made public after our simulations and are not taken into account in our analysis. Nonetheless, they are consistent with our simulations and their interpretations.

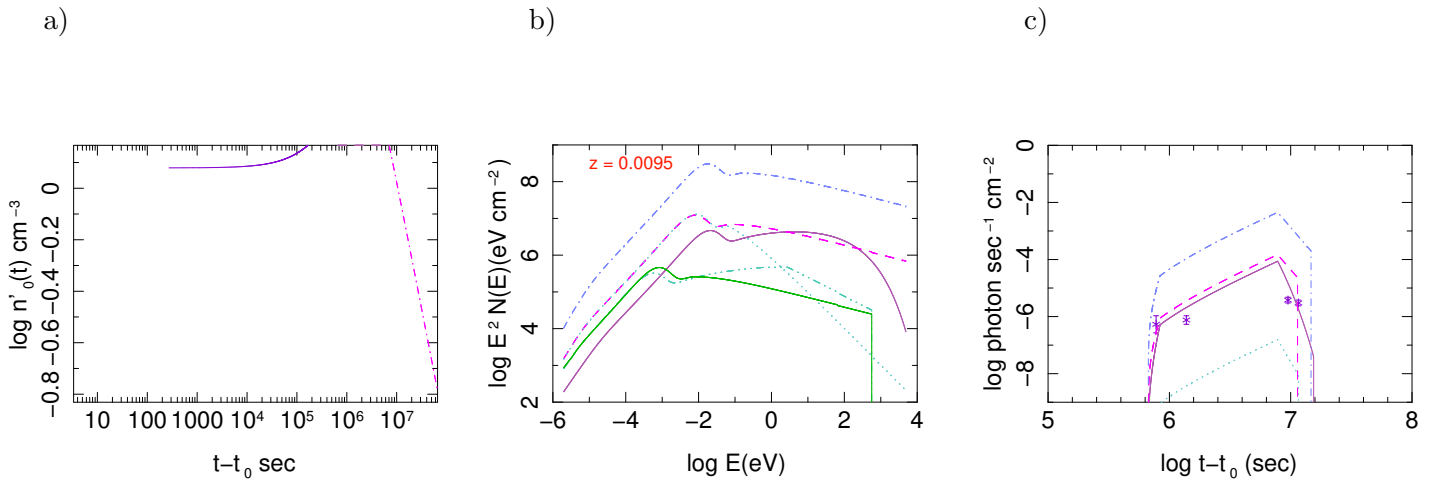


Figure 3. a) Profile of the material sheath around the BNS merger. b) Spectra of simulation No. 2 (dark continuous) and several of its variants with broken power-law spectrum for electrons: $p_2 = 2.5$, $n'_0 = 1 \text{ cm}^{-3}$ and $\Gamma = 3$ (dashed); the same as the previous with $n'_0 = 5 \text{ cm}^{-3}$ (dash-dot); $p_2 = 2.5$ and $n'_c = 5 \times 10^{22} \text{ cm}^{-2}$ (dash-dot); $p_2 = 3$ (dash-3 dot); and $p_2 = 4$, $n'_0 = 1 \text{ cm}^{-3}$ and $\Gamma = 3$ (light continuous). c) X-ray light curves of models in b). The last two models in b) do not have significant emission in this band due to a noticeable break in their spectra at $\sim 0.5 \text{ keV}$ because the simulation code was not able to follow the evolution of rapidly fainting X-ray.

presumably formed during the lifetime of the progenitor neutron stars [80] and its compression in front of the outflow was responsible for generating a density discontinuity and a shock. One may argue that dynamical kick during supernova explosion of the progenitor massive stars might have kicked and ejected the progenitor neutron stars of GW/GRB 170817A event out of their birth place. Although this is a possibility, dynamical kick is not an inevitable outcome of massive stars collapse. Supernova remnants surrounding many neutron stars and pulsars in the Milky Way is an evidence for this fact [41]. Moreover, as the probability of the formation of BNS is higher in star clusters, even a moderate kick might not be sufficient to eject the neutron star out of the potential well of the cluster, which may be dustier than field [11].

Simulations shown in Fig. 1 demonstrate that the density of matter sheath surrounding the BNS at the initial position of the shock front in the simulations must be at least few fold larger than average ISM density of the host galaxy reported in the literature, namely $\sim 0.04 \text{ cm}^{-2}$ - concluded from the absence of significant neutral hydrogen in the host [35]. For lower densities the X-ray flux would be too small.

Although due to simplifications described in Sec. 2 theoretical uncertainties of simulated models may be significant, general aspects of their spectra seem correct, see Fig. 3-b for some examples (and corresponding X-ray light curves in Fig. 3-c). Therefore, it is unlikely that the difficulty of simulations to explain multi-band observations without significant absorption of low energy photons and/or excess of X-ray be simply due to theoretical shortcomings of the model. Indeed, Fig. 3-b shows that for $\Gamma \lesssim 3$, ISM/circumburst density of $\mathcal{O}(1)$, and column density of flow as estimated in Sec. 3.1, the optical/IR band falls in the high energy wing of the spectrum. Thus, the only way to reduce the amount of energy emitted in optical band is to increase the peak energy. This cannot be achieved without much higher Lorentz factor and densities, which are in contradiction with what is expected from a mildly relativistic outflow [65] and a low density ISM/circumburst material, as observations of the host galaxy shows [35].

Irrespective of the results of our simulations, interpretation of multi-band observations as synchrotron or thermal emission would be very difficult without a significant optical/IR extinction or an excess of X-ray emission. Fig. 4 shows the distribution of energy flux density at $\sim T + 110$ days, for which data in all three energy bands discussed here is available. We remind that this distribution is independent of viewing angle and geometry of emitting surface, which are not well understood and are subject to debate and controversies.

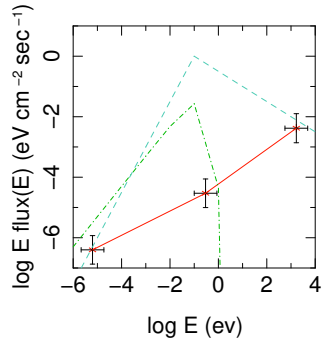


Figure 4. Energy flux distribution of GW/GRB 170817A at $\sim T + 110$ days. Bars on the data points present the width of corresponding energy band rather than measurement errors, which are much smaller. A typical synchrotron spectrum (dashed) is sketched by its asymptotic behaviour with theoretical slope of $3/2$ at low energy wing and a chosen slope of $-1/2$ for high energy wing. Its peak is adjusted to a value close to simulated spectra shown in Fig. 3-b. A thermal spectrum with the same temperature as peak energy of the synchrotron spectrum is also shown (dash-dot). The continuous line connecting data points is drawn as guide for comparison with other curves.

It depends only on the emission mechanism. The observed distribution significantly deviates from a typical synchrotron and thermal spectra shown in Fig. 4 or even a more realistic nonlinear + synchrotron + thermal spectrum simulated by [8, 90]. It is not possible either to assume that all the three energy bands fall on the low energy wing of a synchrotron spectrum, because positive slope of the observed spectrum is much flatter than $3/2$ of synchrotron emission. Moreover, if this assumption were true, the peak of spectrum had to be at even higher energies and the source should have been observable in hard X-ray and gamma-ray.

A large extinction of optical photons is consistent with the fact that optical afterglow of the majority of short bursts are not detected, most probably due to the intrinsic absorption [46, 74]. Assuming that host galaxies of short GRBs have gas column densities comparable to those of Milky Way and NGC4993, their contribution to equivalent N_H should be at most few percent and the rest must be the contribution of immediate environment of source or the outflow itself. On the other hand, the upper limit on the N_H obtained from X-ray observations and its associated extinction are consistent with those of globular clusters, see e.g. [28]. However, multiband observations of NGC 4993 seems to be inconsistent with the presence of a globular or young star cluster with a total mass larger than a few thousands solar masses [51]. Nonetheless, a star cluster dominated by old faint and/or compact stars as the local environment of GW/GRB 170817A event may evade this constraint. For instance, the absolute magnitude limit of $M_V > -6.7$ concluded for any star cluster from observations of [51] is much brighter than the old faint star cluster Segue 3 [24, 37] which has an absolute magnitude of $M \sim 0$ or even a star cluster ~ 400 fold brighter than Segue 3. In addition, a star cluster consisting of an old population as environment of GW/GRB 170817A event is consistent with conclusions obtained from analysis of its prompt gamma-ray emission in [94].

Alternatively, the late afterglow may be the result of multiple collisions between density shells in a mildly relativistic outflow rather than one collision. In this case emissions from shocks occurring closer to the center must pass through the outflow and will be subject to absorption. This scenario is similar to internal shocks in a relativistic jet, but here the flow is only mildly relativistic and shells will need much more time to catch with each other and collide. Our simulations show that in such a model shocks should have properties similar to model No. 3 if only a few shell collisions occurred or model No. 5 if many collisions had taken place. The column densities of these models are consistent with the estimation of N_H in short GRBs [46]. It is also enough to provide the necessary extinction.

In absence of optical/IR extinction an excess of X-ray emission, most probably from kilonova remnant, is necessary to explain the observations. A thermal emission in X-ray from a very hot ejected disk at $\gtrsim T + 100$ seems unlikely. In fact observation of the counterpart in far IR at $\sim T + 264$ days shows that at this epoch the kilonova is cooled and its dominant emission is in far IR [89]. On the other hand, X-ray from decay of nuclides produced in the kilonova and/or recombination of electrons in the ejected disk are credible sources of addition X-ray. Indeed, hundreds of electronic excitation lines and isotopes with half-life of $\mathcal{O}(100)$ days exist, including those related to nuclides produced through r-processes [9].

This alternative solution needs a quantitative investigation, which must include calculation of isotopes yield and their nuclear excitation state in the kilonova and evolution of their ionization state. This task is out of the scope of the present work. Nonetheless, late time X-ray luminosity of GW/GRB 170817A afterglow of $\sim \mathcal{O}(1) \times 10^{39}$ [56] is similar to those of supernovae type II [22]. Although the amount of ejected material from SN type II is much larger than in a BNS merger, most of the material is from the envelop of the star, which has a low level of nuclear excitation. By contrast, BNS ejecta comes from a much denser environment where QCD interaction prevails and includes freshly produced and highly excited isotopes. In addition, GW/GRB 170817A is one of the closest extra-galactic transient ever observed. For instance, it is 3 times closer than type II SN 1988Z which is extensively observed in X-ray [23]. Therefore, radiation from decay of nuclides may have observable contribution.

6 Outlines

In conclusion, shocks generated by the collision of a mildly relativistic outflow with a sheath of material surrounding the merger, or density layers inside the outflow can explain brightening and other characteristics of X-ray, optical/IR, and radio counterparts of GW/GRB 170817A. We suggested two scenarios for the generation of these afterglows.

In the first scenario synchrotron self-absorption and extinction of optical emission in the environment of the source are necessary to explain late multi-band observations. The most probable origin of the external extinction, which may be additionally responsible for the faintness of undetected early afterglow of the GRB 170817A, is the presence of an old star cluster surrounding the progenitor BNS. This conclusion is consistent with larger probability of the formation of BNS and their merger in star clusters than in low density regions of galaxies, and conclusions of [94] from the analysis of prompt gamma-ray emission.

In the second scenario multiple shocks generated by collision of density shells inside the same outflow provide both the emission and absorption of optical emission with respect to X-ray that we find necessary for explaining the data.

An excess of X-ray rather than extinction of optical emission, most probably from decay of nuclides and/or recombination of electrons in the kilonova remnant is another possibility which must be considered and quantified in order to confirm or refute this hypothesis.

Note: After completion of this work, GCN 23137 and GCN 23140 (Haggard, *et al.*), and GCN 23139 (Dobie, *et al.*) reported observations of afterglows of GW/GRB 170817A at $\gtrsim T + 300$ days in X-ray and radio bands, respectively. The observed sharp decline of radio emission at this time is consistent with Simul. No. 6 shown in Fig. 1. Steeper decline of the X-ray light curve and its absorption, which is implicitly an evidence for optical absorption as discussed above are consistent with predictions of this work. Additionally, Mooley *et al.* 2018 (arXiv:1806.09693) report the detection of superluminal motion of a relativistic jet/outflow in VLBI observations. Analysis of this data is consistent with a Lorentz factor of ~ 3 at $\sim T + 150$ days, which is consistent with simulations 1, 6, and two of simulations shown in Fig. 3-b and c.

Acknowledgment: The author thanks the anonymous referee of [94] for encouraging application of [92, 93] model to late afterglows of GW/GRB 170817A.

A Synchrotron self-absorption

Reduction of photon flux of a source due to absorption during propagation of photons in matter is a Possinian process and can be formulated as:

$$\frac{dI_\nu}{d\ell} = \alpha_\nu I_\nu \quad (\text{A.1})$$

where I_ν is intensity at frequency (energy) ν and ℓ is propagation distance inside an absorbing material. For synchrotron self-absorption the absorption coefficient α_ν can be related to distribution of accelerated electrons [75]:

$$\alpha_\omega = \frac{\pi}{2\omega} \int_{\gamma_e}^{\infty} d\gamma_e P(\omega, \gamma_e) \gamma_e^2 \frac{\partial}{\partial \gamma_e} \left(\frac{n'_e(\gamma_e)}{\gamma_e^2} \right) \quad (\text{A.2})$$

where $\omega = E/\hbar$ is photon mode for a photon of energy E ; γ_e is Lorentz factor of accelerated electrons; $n'_e(\gamma_e)$ is number density of electrons with Lorentz factor γ_e ; and $P(\omega, \gamma_e) \equiv dP/\omega d\omega$ is differential synchrotron power density for mode ω .

Using the phenomenological expression of $P(\omega, \gamma_e)$ obtained in [92], the absorption coefficient α_ω can be written as:

$$\alpha_\omega = \frac{\sqrt{3}e^2}{\omega\gamma_m^2} \int_1^{\infty} d\eta F(\eta) \left[\int_{\omega/(\omega_m\eta)}^{\infty} d\zeta K_{5/3}(\zeta) + \dots \right], \quad F(\eta) \equiv \frac{\partial}{\partial \eta} \left(n'_e(\eta) \right) \quad (\text{A.3})$$

where K_ν is the second modified Bessel function of order ν and dots mean higher order subdominant terms which depend on the geometry of the emitting surface. They are neglected in our simulations. This is a good approximation for the prompt emission, in which due to the large Lorentz factor of jet, the effective opening angle visible to a far observer is small and emission is highly beamed. For late afterglows the effect of high latitude emission can be significant and should be added to other uncertainties of the model. In particular, high latitude emission increases the total duration of afterglow for a given detection threshold. Nonetheless, even for a Lorentz factor as small as 2 the visible opening angle is 30° and delay for arrival of photons from high latitudes would be $\sim 13\%$ of the time necessary for light to traverse a distance equal to the radius of emission surface. For an initial distance of $\mathcal{O}(1) \times 10^{16}$ cm used in our simulations and the final radius of ~ 10 times larger, the delay is $\lesssim 10$ days i.e. comparable with the exposure time in the latest observations. Thus, the increase in emission duration due to high latitude emission is of the same order as uncertainty on the observation time and does not have significant impact on the comparison of models with the data.

Equation (A.3) shows that the synchrotron self-absorption coefficient depends on $\eta \equiv \gamma'_e/\gamma'_c$, $\omega'_c \equiv \frac{3e\gamma_e^2 B'_\perp}{2cm_e}$, and $\omega_m = \omega_c|_{\gamma_e=\gamma_m}$ where γ_m is the minimum Lorentz factor of accelerated electrons. The second integral has an approximate analytical expression:

$$\int_{\omega/(\omega_m\eta)}^{\infty} d\zeta K_{5/3}(\zeta) \approx 2K_{2/3}(\omega/(\omega_m\eta)) \quad (\text{A.4})$$

We use this approximate expression in our simulations.

The total amount of synchrotron self-absorption is obtained from integrating eq. (A.1). It depends on the geometric extension of magnetic field in the shock front D_{sy} . In our simulations we assume that this length is proportional to synchrotron characteristic time [75] and reduces exponentially or according to a power-law with propagation of shock front, i.e. $D_{sy}(r) = ct_{sy}(r)f(r/r_0)$ where $t_{sy}(r) = 3c\pi\gamma_m^3(r)/\omega'_c(r)$ is the synchrotron characteristic time for electrons with minimum energy; c is the speed of light. In the simulations we consider either $f(r/r_0) = \exp(-\alpha r/r_0)$ or $f(r/r_0) = (r/r_0)^\alpha$.

B Evolution models of active region

In the phenomenological model of [92] the evolution of $\Delta r'(r')$ cannot be determined from first principles. For this reason we consider the following phenomenological models:

$$\Delta r' = \Delta r'_0 \left(\frac{\gamma'_0 \beta'}{\beta'_0 \gamma'} \right)^\tau \Theta(r' - r'_0) \quad \text{dynamical model, Model} = 0 \quad (\text{B.1})$$

$$\Delta r' = \Delta r'_\infty \left[1 - \left(\frac{r'}{r'_0} \right)^{-\delta} \right] \Theta(r' - r'_0) \quad \text{Steady state model, Model} = 1 \quad (\text{B.2})$$

$$\Delta r' = \Delta r'_0 \left(\frac{r'}{r'_0} \right)^{-\delta} \Theta(r' - r'_0) \quad \text{Power-law model, Model} = 2 \quad (\text{B.3})$$

$$\Delta r' = \Delta r_\infty \left[1 - \exp\left(-\frac{\delta(r' - r'_0)}{r'_0}\right) \right] \Theta(r' - r'_0) \quad \text{Exponential model, Model} = 3 \quad (\text{B.4})$$

$$\Delta r' = \Delta r'_0 \exp\left(-\delta \frac{r'}{r'_0}\right) \Theta(r' - r'_0) \quad \text{Exponential decay model, Model} = 4 \quad (\text{B.5})$$

The initial width $\Delta r'(r'_0)$ in Model = 1 & 3 is zero. Therefore, they are suitable for description of initial formation of an active region in internal or external shocks. Other models are suitable for describing more moderate growth or decline of the active region. In Table 2 the column *mod.* indicates which evolution rule is used in a simulation regime - as defined in the foot notes of this table - using model number given in B.1-B.5.

References

- [1] Alexander, K.D., Berger, E., Fong, W., Williams, P.K.G., Guidorzi, C., Margutti, R., Metzger, B.D., Annis, J., *et al.*, *ApJ.Lett.* **848**, (2017) L21 [[arXiv:1710.05457](#)].
- [2] Alexander, K.D., Margutti, R., Blanchard, P.K., Fong, W., Berger, E., Hajela, A., Eftekhari, T., Chornock, R., *et al.*, (2018) [[arXiv:1805.02870](#)].
- [3] Arcavi, I., Hosseinzadeh, G., Howell, D.A., McCully, C., Poznanski, D., Kasen, D., Barnes, J., Zaltzman, M., Vasylyev, S., Maoz, D., Valenti, S., *Nature* **551**, (2017) 64 [[arXiv:1710.05843](#)].
- [4] Levinson, A., Begelman, M.C., *ApJ.* **764**, (2013) 148 [[arXiv:1209.5261](#)].
- [5] Berger, E., Fong, W., Chornock, R., *ApJ.Lett.* **774**, (2013) L23 [[arXiv:1306.3960](#)].
- [6] Bromberg, O., Tchekhovskoy, A., *MNRAS* **456**, (2016) 1739 [[arXiv:1508.02721](#)].
- [7] Burgala, L.F., Ness, N.F., Acuna, M.H., Lepping, R.P., Connerney, J.E.P., Richardson, J.D., *Nature* **454**, (2008) 75.
- [8] Burgess, J.M., Preece, R.D., Connaughton, V., Briggs, M.S., Goldstein, A., Bhat, P.N., Greiner, J., Gruber, D., *et al.*, *ApJ.* **784**, (2014) 17 [hrefhttps://arxiv.org/abs/1304.4628](https://arxiv.org/abs/1304.4628)[[arXiv:1304.4628](#)].
- [9] Chu, S.Y.F., Ekstrm1, L.P., Firestone, R.B., “The Lund/LBNL Nuclear Data Search”, <http://nucleardata.nuclear.lu.se/toi/>.
- [10] Church, R.P., Levan, A.J., Davies, M.B., Tanvir, N., in proceedings of “GRBs as probes: from the progenitor’s environment to the high redshift Universe”, Como, Italy, May 2011, [[arXiv:1110.4209](#)].
- [11] Michelle Consiglio, S., Turner, J.L., Beck, S., Meier, D., *ApJ.Lett.* **835**, (2016) L6 [[arXiv:1611.09936](#)].
- [12] Covino, S., Wiersema, K., Z.Fan, Y., Toma, K., B.Higgins, A., Melandri, A., D’Avanzo, P., G.Mundell, C., *et al.*, *Nature Astro.* **1**, (2017) 791 [[arXiv:1710.05849](#)].
- [13] Coulter, D.A., Foley, R.J., Kilpatrick, C.D., Drout, M.R., Piro, A.L., Shappee, B.J., Siebert, M.R., Simon, J.D., *et al.*, *Science* **358**, (2017) 1556 [[arXiv:1710.05452](#)].
- [14] Cowperthwaite, P.S., Berger, E., Villar, V.A., Metzger, B.D., Nicholl, M., Chornock, R., Blanchard, P.K., Fong, W., *et al.*, *ApJ.Lett.* **848**, (2017) 17 [[arXiv:1710.05840](#)].

- [15] Cummings, J.R., Barthelmy, S.D., Gronwall, C., Holland, S.T., Kennea, J.A., Marshall, F.E., Palmer, D.M., Perri, *et al.*, M., (2006) *GCN Circ.* **5301**.
- [16] De Colle, F., Lu, W., Kumar, P., Ramirez-Ruiz, E., Smoot, G., (2017) [[arXiv:1701.05198](#)].
- [17] D’Avanzo, P., Campana, S., Ghisellini, G., Melandri, A., Bernardini, M.G., Covino, S., D’Elia, V., Nava, L., *et al.*, *A. & A.* **613**, (2018) L1 [[arXiv:1801.06164](#)].
- [18] De Pasquale, M., Barthelmy, S.D., Campana, S., Cummings, J.R., Godet, O., Guidorzi, C., Hill, J.E., Holland, S.T., Kennea, J.A., *et al.*, (2006) *GCN Circ.* **5409**
- [19] Dingus B.L., *Space Sci.* **231**, (1995) 187
- [20] Dionysopoulou, K., Alic, D., Rezzolla, L., *Phys. Rev. D* **92**, (2015) 084064 [[arXiv:1502.02021](#)].
- [21] Dobie, D., Kaplan, D.L., Murphy, T., Lenc, E., Mooley, K.P., Lynch, C., Corsi, A., Frail, D., Kasliwal, M., Hallinan, G., *ApJ.* **858**, (2018) L15 [[arXiv:1803.06853](#)].
- [22] Dwarkadas, V.V., Gruszko, J., *MRA* **0419**, (2012) 1515 [[arXiv:1109.2616](#)].
- [23] Fabian, A.C., Terlevich R., *MNRAS* **280**, (1996) L5 [[astro-ph/9511060](#)].
- [24] Fadely, R., Willman, B., Geha, M., Walsh, S., Munoz, R.R., Jerjen, H., Vargas, L.C., Da Costa, G.S., *Astron. J.* **142**, (2011) 88 [[arXiv:1107.3151](#)].
- [25] Fargion, D., Khlopov, M., Oliva, P., *Int. J. Mod. Phys. D* **27**, (2018) 1841001 [[arXiv:1710.05909](#)].
- [26] Fong, W.F., Berger, E., Metzger, B.D., Margutti, R., Chornock, R., Migliori, G., Foley, R.J., Zauderer, B.A., *et al.*, *ApJ.* **780**, (2013) 118 [[arXiv:1309.7479](#)].
- [27] Foucart, F., Desai, D., Brege, W., Duez, M.D., Kasen, D., Hemberger, D.A., Kidder, L.E., Pfeiffer, H.P., Scheel, M.A., *Class.Quant.Grav.* **34**, (2017) 044002 [[arXiv:1611.01159](#)].
- [28] Froebrich, D., Rowles, J., *MNRAS* **406**, (2010) 1350 [[arXiv:1004.0117](#)].
- [29] Gehrels, N., Chincarini, G., Giommi, P., Mason, K.O., Nousek, J.A., Wells, A.A., White, N.E., Barthelmy, S.D., *et al.*, *ApJ.* **611**, (2004) 1005 [[astro-ph/0405233](#)].
- [30] Gill, R., Granot, J., *MNRAS* **sty1214**, (2018) [[arXiv:1803.05892](#)].
- [31] Goldstein, A., Veres, P., Burns, E., Briggs, M.S., Hamburg, R., Kocevski, D., Wilson-Hodge, C.A., Preece, R.D., *ApJ.Lett.* **848**, (2017) L14 [[arXiv:1710.05446](#)].
- [32] Gorenstein, P., *ApJ.* **198**, (1975) 95.
- [33] Gottlieb, O., Nakar, E., Piran, T., Hotokezaka, K., (2017) [[arXiv:1710.05896](#)].
- [34] Güver, T., Özel, F., *MNRAS* **400**, (2009) 2050 [[arXiv:0903.2057](#)].
- [35] Hallinan, G., Corsi, A., P.Mooley, K., Hotokezaka, K., Nakar, E., Kasliwal, M.M., Kaplan, D.L., Frail, D.A., *et al.*, *Science* **358**, (2017) 1579 [[arXiv:1710.05435](#)].
- [36] Hotokezaka, K., Kiuchi, K., Shibata, M., Nakar, E., Piran, T., (2018) [[arXiv:1803.00599](#)].
- [37] Hughes, J., Lacy, B., Sakari, C., Wallerstein, G., Evan Davis, C., Schiefelbein, S., Corrin, O., Joudi, H., Le, D., Haynes, R.M., *Astron. J.* **154**, (2017) 57 [[arXiv:1706.01961](#)].
- [38] Kann D.A., *EAS Publications Series* **61**, (2013) 309 [[arXiv:1212.0040](#)].
- [39] Kasen, D., Metzger, B., Barnes, J., Quataert, E., Ramirez-Ruiz, E., *Nature* **551**, (2017) 80 [[arXiv:1710.05463](#)].
- [40] Kasliwal, M.M., Nakar, E., Singer, L.P., Kaplan, D.L., Cook, D.O., Van Sistine, A., Lau, R.M., *et al.*, *Science* **358**, (2017) 1559 [[arXiv:1710.05436](#)].
- [41] Kaspi, V.M., Manchester, R.N., Johnston, S., Lyne, A.G., D’Amico, N., *Astron. J.* **111**, (1996) 2028.
- [42] Kathirgamaraju, A., Barniol Duran, R., Giannios, D., *MNRAS* **473**, (2018) L121 [[arXiv:1708.07488](#)].
- [43] Kisaka, S., Ioka, K., Kashiyama, K., Nakamura T., (2017) [[arXiv:1711.00243](#)].
- [44] Kiuchi, K., Kyutoku, K., Sekiguchi, Y., Shibata, M., Wada, T., *Phys. Rev. D* **90**, (2014) 041502 [[arXiv:1407.2660](#)].
- [45] Komissarov, S., Vlahakis, N., Konigl, A., Barkov, M., *MNRAS* **394**, (2009) 1182 [[arXiv:0811.1467](#)].

- [46] Kopac, D., D’Avanzo, P., Melandri, A., Campana, S., Gomboc, A., Japelj, J., Bernardini, M.G., Covino, S., *et al.*, *MNRAS* **424**, (2012) 2392 [[arXiv:1203.1864](#)].
- [47] Lamb, G.P., Kobayashi, S., *MNRAS* **472**, (2017) 4953 [[arXiv:1706.03000](#)].
- [48] Lazzati, D., Deich, A., Morsony, B.J., Workman, J.C., *MNRAS* **471**, (2017) 1652 [[arXiv:1610.01157](#)].
- [49] Lazzati, D., Perna, R., Morsony, B.J., López-Cmara, D., Cantiello, M., Ciolfi, R., Giacomazzo, B., Workman, J.C., (2017) [[arXiv:1712.03237](#)].
- [50] Lee, W.H., Ramirez-Ruiz, E., van de Ven, G., *ApJ*. **720**, (2010) 953 [[arXiv:0909.2884](#)].
- [51] Levan, A.J., Lyman, J.D., Tanvir, N.R., Hjorth, J., Mandel, I., Stanway, E.R., Steeghs, D., Fruchter, A.S., Troja, E., *et al.*, *ApJ.Lett.* **848**, (2017) L12 [[arXiv:1710.05444](#)].
- [52] Li, B., Li, L.B., Huang, Y.F., Geng, J.J., Yu, Y.B., Song L.M., *ApJ.Lett.* **859**, (2018) L3 [[arXiv:1802.10397](#)].
- [53] Lyman, J.D., Lamb, G.P., Levan, A.J., Mandel, I., Tanvir, N.R., Kobayashi, S., Gompertz, B., Hjorth, *et al.*, J., (2017) [[arXiv:1801.02669](#)].
- [54] Mandel, I., *ApJ*. **853**, (2018) L12 [[arXiv:1712.03958](#)].
- [55] Margutti, R., Berger, E., Fong, W., Guidorzi, C., Alexander, K.D., Metzger, B.D., Blanchard, P.K., Cowperthwaite, P.S., *et al.*, *ApJ.Lett.* **848**, (2017) L20 [[arXiv:1710.05431](#)].
- [56] Margutti, R., Alexander, K.D., Xie, X., Sironi, L., Metzger, B.D., Kathirgamaraju, A., Fong, W., Blanchard, P.K., Berger, *et al.*, E., (2017) [[arXiv:1801.03531](#)].
- [57] Melandri, A., Baumgartner, W.H., Burrows, D.N., Cummings, J.R., Gehrels, N., Gronwall, C., Page, K.L., M.Palmer, *et al.*, D., (2013) *GCN Circ.* **14735**.
- [58] Meng, Y-Z., Geng, J-J., Zhang, B-B., Wei, J-J., Xiao, D., Liu, L-D., Gao, H., Wu, X-F., *et al.*, *ApJ*. **860**, (2018) 72 [[arXiv:1801.01410](#)].
- [59] Metzger, B.D., Thompson, T.A., Quataert, E., *ApJ*. **856**, (2018) 101 [[arXiv:1801.04286](#)].
- [60] Mooley, K.P., Nakar, E., Hotokezaka, K., Hallinan, G., Corsi, A., Frail, D.A., Horesh, A., Murphy, T., Lenc, E., *et al.*, *Nature* **554**, (2018) 207 [[arXiv:1711.11573](#)].
- [61] Murase, K., Toomey, M.W., Fang, K., Oikonomou, F., Kimura, S.S., Hotokezaka, K., Kashiyama, K., Ioka, K., Meszaros, P., (2017) [[arXiv:1710.10757](#)].
- [62] Murguia-Berthier, A., Ramirez-Ruiz, E., Kilpatrick, C.D., Foley, R.J., Kasen, D., Lee, W.H., Piro, A.L., Coulter, D.A., *et al.*, *ApJ.Lett.* **848**, (2017) L34 [[arXiv:1710.05453](#)].
- [63] Nakar, E., Sari, R., *ApJ*. **747**, (2012) 88 [[arXiv:1106.2556](#)].
- [64] Nakar, E., Piran, T., *ApJ*. **834**, (2016) 28 [[arXiv:1610.05362](#)].
- [65] Nakar, E., Gottlieb, O., Piran, T., Kasliwal, M.M., Hallinan G., (2018) [[arXiv:1803.07595](#)].
- [66] Nicholl, M., Berger, E., Kasen, D., D.Metzger, B., Elias, J., Briceno, C., D.Alexander, K., K.Blanchard, P., *et al.*, *ApJ.Lett.* **848**, (2017) 18 [[arXiv:1710.05456](#)].
- [67] Nynka, M., Ruan, J.J., Haggard, D., (2018) [[arXiv:1805.04093](#)].
- [68] Oates, S.R., Barthelmy, S.D., Baumgartner, W.H., Beardmore, A.P., Evans, P.A., Gehrels, N., Holland, S.T., Kennea, *et al.*, J.A., (2009) *GCN Circ.* **10148**.
- [69] Pian, E., D’Avanzo, P., Benetti, S., Branchesi, M., Brocato, E., Campana, S., Cappellaro, E., Covino, S., *et al.*, *Nature* **551**, (2017) 67 [[arXiv:1710.05858](#)].
- [70] Piro, L., Troja, E., Gendre, B., Ghisellini, G., Ricci, R., Bannister, K., Fiore, F., Kidd, L.A., *et al.*, *ApJ.Lett.* **790**, (2014) 15 [[arXiv:1405.2897](#)].
- [71] Predehl, P., Schmitt, J.H.M.M., *A.&A.* **293**, (1995) 889.
- [72] Pozanenko, A., Barkov, M.V., Minaev, P.Y., Volnova, A.A., Mazaeva, E.D., Moskvitin, A.S., Krugov, M.A., Samodurov, *et al.* V.A., (2017) [[arXiv:1710.05448](#)].
- [73] Reina, C., Tarenghi, M., *A.&A.* **26**, (1973) 257.
- [74] Roming, P.W.A., Koch, T.S., Oates, S.R., Porterfield, B.L., Vanden Berk, D.E., Boyd, P.T., Holland, S.T.,

- Hoversten, E.A., *et al.*, *ApJ*. **690**, (2009) 163 [[arXiv:0809.4193](#)], [Version 2](#).
- [75] Rybicki, G.B., Lightman, A.P., 2004, "Radiative Processes in Astrophysics", Wiley-VCH verlag GmbH & Co.KGAA, Weinheim.
- [76] Salafia, O.S., Ghisellini, G., Ghirlanda, G., Colpi M., (2017) [[arXiv:1711.03112](#)].
- [77] Sari, R., Piran, T., *ApJ*. **455**, (1995) L143 [astro-ph/9508081](#).
- [78] Sari, R., Narayan, R., Piran, T., *ApJ*. **473**, (1996) 204 [astro-ph/9605005](#).
- [79] Savchenko, V., Ferrigno, C., Kuulkers, E., Bazzano, A., Bozzo, E., Brandt, S., Chenevez, J., Courvoisier, T.J.-L., *et al.*, *ApJ.Lett.* **848**, (2017) L15 [[arXiv:1710.05449](#)].
- [80] Slane P., in "Handbook of Supernovae" (2017), 2159, Eds. A.W. Alsabti, P. Murdin, Springer, Cham [[arXiv:1703.09311](#)].
- [81] Smartt, S.J., Chen, T.W., Jerkstrand, A., Coughlin, M., Kankare, E., Sim, S.A., Fraser, M., Inserra, C., *et al.*, *Nature* **551**, (2017) 75 [[arXiv:1710.05841](#)].
- [82] Soares-Santos, M., Holz, D.E., Annis, J., Chornock, R., Herner, K., Berger, E., Brout, D., Chen, H., *et al.*, *ApJ.Lett.* **848**, (2017) L16 [[arXiv:1710.05459](#)].
- [83] Spitkovsky, A., *ApJ*. **682**, (2008) 5 [[arXiv:0802.3216](#)].
- [84] Tanabashi, M., *et al.*, *Phys. Rev. D* **98**, (2018) 030001 ([Particle Data Group](#)).
- [85] Tanvir, N.R., Levan, A.J., Fruchter, A.S., Hjorth, J., Hounsell, R.A., Wiersema, K., Tunnicliffe, R., *Nature* **500**, (2013) 547 [[arXiv:1306.4971](#)].
- [86] Tchekhovskoy, A., McKinney, J.C., Narayan, R., *MNRAS* **388**, (2008) 1365 [[arXiv:0803.3807](#)].
- [87] Troja, E., Piro, L., van Eerten, H., Wollaeger, R.T., Im, M., Fox, O.D., Butler, N.R., Cenko, S.B., *et al.*, *Nature* **551**, (2017) 71 [[arXiv:1710.05433](#)].
- [88] Troja, E., Piro, L., Ryan, G., van Eerten, H., Ricci, R., Wieringa, M., Lotti, S., Sakamoto, T., Cenko, S.B., (2018) [[arXiv:1801.06516](#)].
- [89] Villar, V.A., Cowperthwaite, P.S., Berger, E., Blanchard, P.K., Gomez, S., Alexander, K.D., Margutti, R., Chornock, R., *et al.*, (2018) [arXiv:1805.08192](#).
- [90] Warren, D.C., Ellison, D.C., Barkov, M.V., Nagataki S., *ApJ*. **835**, (2017) 248 [[arXiv:1701.04170](#)].
- [91] Willingale, R., O'Brien, P., Osborne, J.P., Godet, O., Page, K.L., Goad, M.R., Burrows, D.N., Zhang, B., Rol, E., Gehrels, N., Chincarini, G., *ApJ*. **662**, (2007) 1093 [[astro-ph/0612031](#)].
- [92] Ziaepour, H., *MNRAS* **397**, (2009) 361 [[arXiv:0812.3277](#)].
- [93] Ziaepour, H., Gardner, B., *J. Cosmol. Astrop. Phys.* **12**, (2011) 001 [[arXiv:1101.3909](#)].
- [94] Ziaepour H., *MNRAS* **478**, (2018) 3233 [[arXiv:1801.06124](#)].